
Correction and Characterization of Scattered Events in Three-Dimensional PET Using Scanners with Retractable Septa

Simon R. Cherry, Steven R. Meikle and Edward J. Hoffman

The Crump Institute and the Division of Nuclear Medicine and Biophysics, UCLA School of Medicine, Los Angeles, California and Department of Nuclear Medicine, Royal Prince Alfred Hospital, Sydney, Australia

Large sensitivity increases are realized in positron emission tomography when the interplane septa are removed and all lines of response acquired. Unfortunately, three-dimensional acquisition results in a large increase in scatter fraction which prevents accurate quantitation. By acquiring short two-dimensional scans prior to three-dimensional ones, scatter distributions can be estimated from differences between lines of response common to both datasets. This initial scatter distribution can be further modified to approximate scatter in the entire three-dimensional dataset. The method was validated with phantom measurements in which absolute activity concentrations were known in all compartments. Following scatter correction, a four-compartment phantom that was nonuniform in activity and density, both axially and transversally, gave activity concentrations of 0.45 ± 0.02 , 0.31 ± 0.02 , 0.01 ± 0.01 and 0.01 ± 0.01 $\mu\text{Ci/cc}$ for compartments containing 0.43, 0.29, 0.0 (air) and 0.0 (water) $\mu\text{Ci/cc}$, respectively. Thus, scatter distributions for complex sources can be estimated from image data without lengthy Monte-Carlo simulations. When activity distributions vary slowly with time, this method can be used to correct for scatter in three-dimensional patient studies.

J Nucl Med 1993; 34:671-678

Positron emission tomography (PET) studies are generally count-limited and greatly benefit from the large increase in sensitivity realized by retracting the interplane septa and acquiring all possible coincidence lines of response (LORs) (1-3). Unfortunately, this approach also leads to increases in the scatter fraction which degrades image contrast and adversely affects both relative and absolute quantitation. Methods for characterizing and correcting for scatter are therefore necessary before three-dimensional data acquisition can be routinely employed across a wider spectrum of PET studies. Cur-

rently, attention is focused on scatter removal from emission studies since scatter-free transmission scans can, in principle, be obtained using a rotating rod source with windowed data acquisition (4). Alternatively, scatter-free attenuation correction factors (ACFs) for brain studies can be obtained using a calculated attenuation correction based on edge detection in the sinograms (5,6).

A major problem in developing and testing scatter correction algorithms is that the scatter distribution for realistic sources and scattering media is not known. The scatter distribution from simple source configurations can be simulated by Monte-Carlo techniques, but this is a slow, computer intensive procedure which requires accurate modeling of the PET system (7-9). We have developed a new method which utilizes an additional short data acquisition with septa in place and uses the difference between this two-dimensional study and the three-dimensional one to define the scatter distribution. This technique, the difference method, allows scatter distributions for complex source and density distributions to be measured experimentally in a few minutes. It also provides information which will be useful in characterizing the scatter distribution over a wide range of realistic imaging conditions. It will be particularly useful for assessing other scatter correction methods in a more direct fashion. In a wide range of applications, the activity distribution varies slowly with time and the difference method can be used to perform the actual scatter correction for three-dimensional patient studies.

Scatter correction of three-dimensional PET datasets is currently being pursued by a number of groups. The most promising approaches include an extension of the two-dimensional deconvolution method (10) to a three-dimensional one using an iterative approach (11,12) and simultaneous measurement in a second energy window (13). These approaches, however, rely on a certain amount of empirical information, such as the shape of line spread functions or the ratio of scattered events in pairs of energy windows which are assumed to be valid for all or most source distributions. Additionally, with the dual-energy method, the relatively large three-dimensional

Received Sept. 17, 1992; revision accepted Dec. 2, 1992.
For reprints or correspondence contact: Simon R. Cherry, Division of Nuclear Medicine & Biophysics, UCLA School of Medicine, Los Angeles, CA 90024-1721.

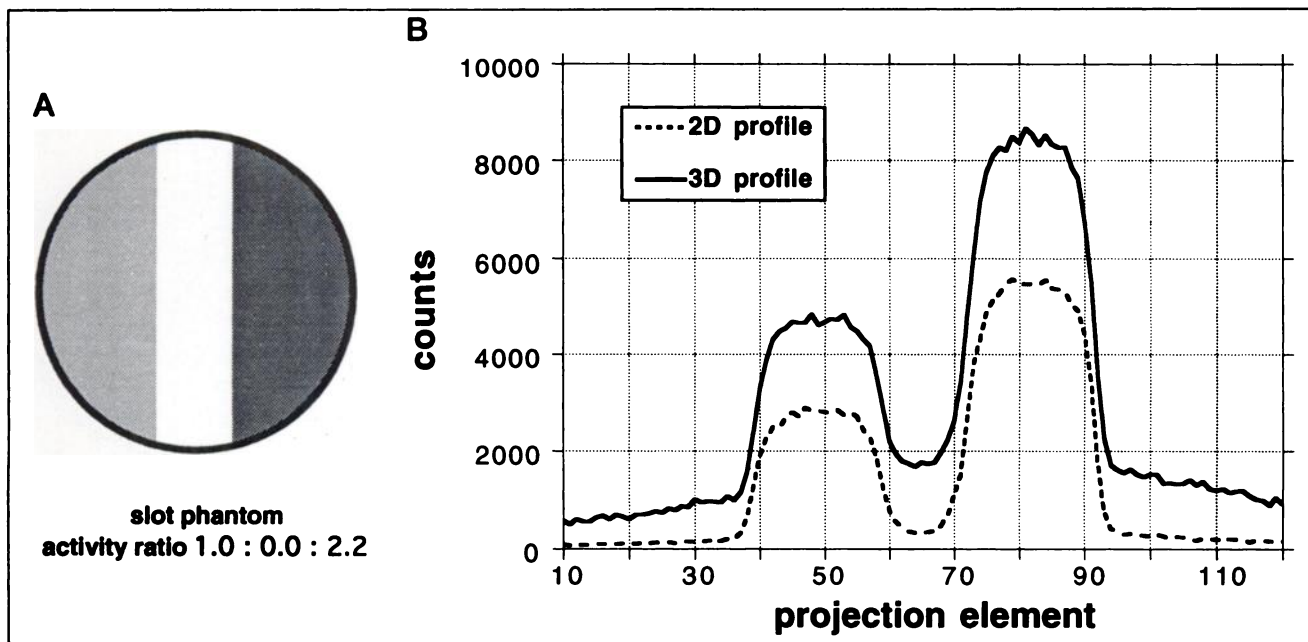


FIGURE 1. (A) Configuration of slot phantom used to illustrate the difference method. The ratio of activity in the phantom was 1:0:2.2. (B) Decay-corrected projections through sequential two-dimensional and three-dimensional acquisitions of slot phantom data. Notice the increased scatter fraction and increased efficiency in the three-dimensional projections.

dataset is doubled. Because of the assumptions involved, these methods apparently work satisfactorily for uniform attenuation media, but may have problems with highly asymmetric activity or density distributions. Another approach is to use analytical expressions combined with emission and transmission data to estimate the scatter distribution (14,15). The challenge in this case is to make the computation rapid while retaining sufficient accuracy in the resulting scatter distribution. One drawback of this method is that it cannot account for scatter from activity outside of the field of view.

The technique we propose makes few assumptions and incorporates no empirical information. As such, it should be a useful tool for objectively assessing a range of three-dimensional scatter correction methods. It may also become a scatter correction method in itself for those studies which satisfy the criteria required for accurate correction.

METHOD DESCRIPTION

All coincidence lines of response (LORs) acquired in a two-dimensional PET study are also acquired as part of the three-dimensional dataset. In particular, LORs corresponding to direct-plane coincidences (i.e., ring difference = 0) are measured in both two-dimensions and three-dimensions. Assuming the isotope distribution remains constant, the difference in counts registered in sequential decay-corrected two- and three-dimensional acquisitions of these LORs will be due to increased efficiency (removal of septa-shadowing effect) and the increase in the number of scattered events detected. If one can correct for the efficiency differences, the remaining difference will be due solely to scattered events. The aim of this study was to determine if this difference could be exploited to give an accurate

measure of the scatter distribution in three-dimensional PET studies, potentially leading to a simple, experimental scatter correction method.

The method is illustrated using a single one-dimensional projection from a slot phantom, which has three compartments containing activity in the ratio 2.2:0:1 (Fig. 1A). The data were acquired on the ECAT-831 tomograph (CTI/Siemens, Knoxville, TN), an eight ring scanner (320 detectors/ring) with a ring diameter of 64 cm and an axial field of view of 10.8 cm (16,17). The energy window was 250–850 keV, the routine setting for studies on this system. Characterization of this scanner for three-dimensional acquisition has been previously reported (3). Two- and three-dimensional projection data from coincidences within a single detector ring across the slot phantom are shown in Figure 1B. The presence of scatter in the central cold compartment and in the projection wings is particularly evident in the three-dimensional projection. Note also the higher efficiency of the three-dimensional study.

Efficiency Correction

Correction factors for the efficiency differences between two- and three-dimensional studies can be obtained by taking the ratio of scatter-free blank scans obtained with a rotating rod source. The scatter contribution, S' , for each LOR element (r, θ) is then calculated for all direct plane (i.e., ring difference = 0) sinograms according to:

$$S'(r, \theta) = C_{3D}(r, \theta) - \epsilon(r, \theta)C_{2D}(r, \theta), \quad \text{Eq. 1}$$

where $\epsilon(r, \theta)$ are the efficiency correction factors for each LOR and C_{2D} and C_{3D} are the LOR counts in the two- and three-dimensional study respectively. Figure 2 shows the scatter projection calculated using Equation 1 and the original three-dimensional projection data for comparison. The scatter profile contains only low frequencies (except for noise), which is to be

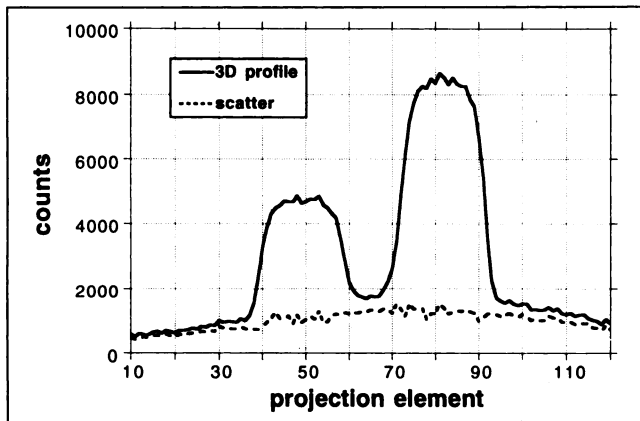


FIGURE 2. Three-dimensional projection and first estimate of scatter distribution (based on subtraction of efficiency corrected two-dimensional projection data) from slot phantom. The scatter in the projection tails and in the central compartment is underestimated due to the scatter originally in the two-dimensional dataset.

expected given the broad nature of the scatter distribution and the comparatively poor energy resolution of PET. Several Monte Carlo studies (7,9) have shown that there is only a very weak correlation between activity distribution and scatter distribution. No structure therefore is expected in the scatter profiles even for quite asymmetrical source distributions. Given this, the smoothness of the scatter profile across discontinuities in activity provides evidence that the efficiency correction is accurate. The scatter distribution also exhibits the correct general shape when compared to the projection wings and the cold compartment. However, it clearly underestimates the total scatter. This would be expected, since the two-dimensional study also contains non-negligible amounts of scatter, and the correction so far only takes into account the extra scatter in going from two-dimensional acquisition to three-dimensional acquisition.

Correcting for Scatter in the Two-Dimensional Study

In order to correct for the residual scatter present in the two-dimensional data, we hypothesize that the total scatter distribution $S(r, \theta)$ can be obtained by simply scaling the scatter distribution $S'(r, \theta)$ obtained from Equation 1 for each one-dimensional projection to achieve equal counts in the scatter tails outside the object. Given the relatively small axial acceptance angles of multi-slice tomographs (usually $<10^\circ$), this is unlikely to be a bad approximation. Fortunately, it can be tested directly. First, the slot phantom is considered. For LORs which contain only scattered events (the projection wings and central cold compartment), the ratio of the three-dimensional projection to the estimated scatter projection should equal a constant if our hypothesis is valid. Figure 3 shows a plot of this ratio which illustrates that the ratio in the projection wings and the central compartments are not significantly different from each other.

Additional support for the hypothesis comes from imaging an offcenter (both axially and radially) ^{68}Ge line source (1 mm diameter) in an 18-cm diameter cold cylinder (Fig. 4). The total scatter in LOR (r, θ) is given by:

$$S(r, \theta) = k(\theta)S'(r, \theta), \quad \text{Eq. 2}$$

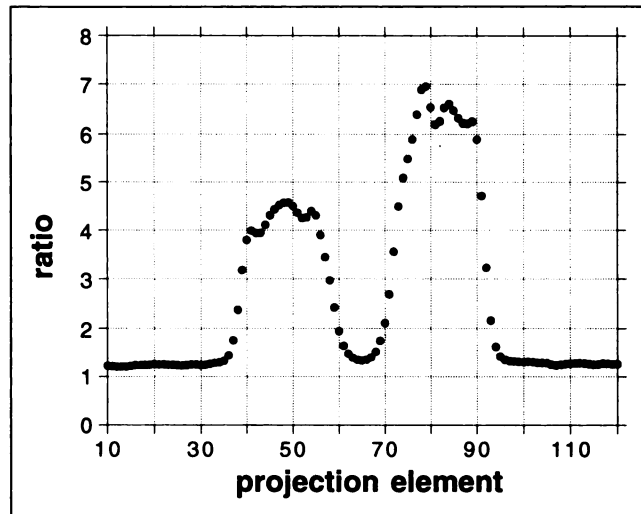


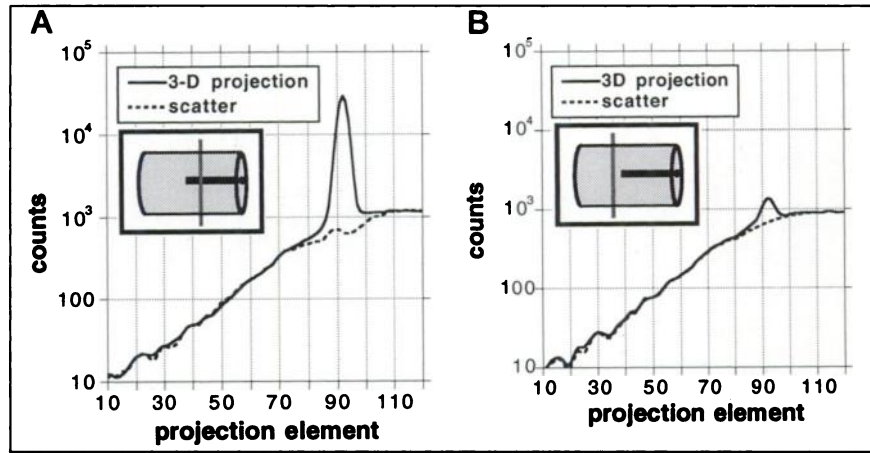
FIGURE 3. Ratio of three-dimensional projection data over scatter estimate S' . The constant value of this ratio in regions which only contain scattered events (projection wings and central compartment) supports the use of a simple scaling factor to convert S' to the total scatter distribution S .

where $k(\theta)$ is the ratio of counts in the projection wings between the three-dimensional projection and S' for a given angle. The estimated scatter distribution, S , for a projection containing the line source (Fig. 4A), and for a projection just beyond the axial extent of the line source (Fig. 4B) was compared with the measured projection and showed very close agreement across the whole projection.

The outcome is that for a given direct plane sinogram, the scaling factor k is independent (s.d./mean $<2\%$) of the projection angle θ (Fig. 5). This leads to a considerable simplification of the method and does not require that substantial scatter tails be present in every projection in order to estimate k . In the axial direction, however, there are significant changes in k due to the faster drop in scatter magnitude of three-dimensional datasets compared with two-dimensional datasets towards the axial extremes of the scanner (Fig. 5). Thus, k must be computed separately for each direct plane sinogram. These results, using a highly asymmetric source distribution, indicate that using a scaling factor to account for the scatter originally in the two-dimensional study is a reasonable assumption for our particular scanner geometry. In distributed sources, the errors are likely to be even smaller. However, this assumption may prove less satisfactory for scanners with wider acceptance angles or for narrowly defined energy windows.

The calculated scatter distribution for the slot phantom projection (after efficiency correction and scaling for two-dimensional scatter) is shown in Figure 6. The fit to the tails of the projection and central cold compartment components of the three-dimensional projection are excellent. By performing the efficiency correction for each projection element and applying the scaling factor to account for scatter in the two-dimensional scan, the scatter distribution $S(r, \theta)$ can be obtained for all direct-plane sinograms. This in itself is useful for defining the scatter distribution but in order to be useful as a scatter correction, it will be necessary to extend the scatter distribution into the obliquely oriented projections which form the remainder of the three-dimensional dataset.

FIGURE 4. One millimeter diameter line source, 8 cm radial displacement, placed inside an 18-cm diameter cylinder. (A) Projection data and calculated scatter distribution for line of response passing through line source. (B) Projection data and calculated scatter distribution for line of response passing 8 mm (axially) outside the source position. Note the excellent fit of the estimated scatter distribution to the measured data in both cases.



Extension of Scatter Distribution to Oblique Projections

Given the low spatial frequencies of scatter in PET, we expect scatter distributions in closely adjacent LORs to be very similar. We can use this principle to extend the scatter distribution to the oblique LORs when the acceptance angle is not too large. For example, in the ECAT-831, the LORs corresponding to coincidences between ring 1 and 7 form an angle of only 7° with the corresponding LORs in direct plane sinogram 4. Assuming that the shape of the scatter distribution does not change over this small angle, each oblique scatter sinogram (ring indices n , m) is calculated from the corresponding direct plane sinograms (ring index k) intersecting the plane of interest according to:

$$S_{nm}(r, \theta) = A\{w_1 S_k(r, \theta) + w_2 S_{k+1}(r, \theta)\}, \quad \text{Eq. 3}$$

where $k = \text{int}(n+m/2)$, $w_2 = (n+m/2) - \text{int}(n+m/2)$ and $w_1 = 1 - w_2$. A is a scaling constant allowing the magnitude (but not the

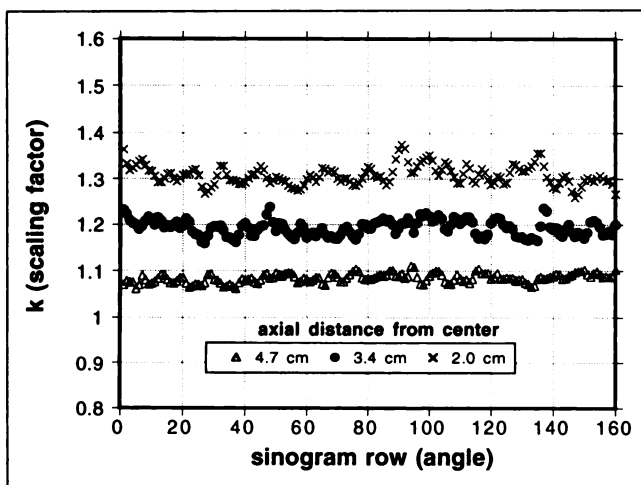


FIGURE 5. Variation of scaling factor k as a function of sinogram row (projection angle θ) and axial distance from center of tomograph for data from slot phantom. Mean and standard deviations are 1.08 ± 0.01 at 5.4 cm, 1.19 ± 0.02 at 3.4 cm, 1.31 ± 0.02 at 2.0 cm and 1.34 ± 0.03 at 0.7 cm (not shown). These plots show that k is independent of the projection angle θ , but is sensitive to variations in axial distance.

shape) of the scatter distribution to vary in the oblique LORs. This parameter is found once again by fitting the projection wings.

Finally, the estimated three-dimensional scatter distribution is heavily smoothed (using a Gaussian of FWHM 25 mm) to minimize the propagation of noise upon its subtraction from the measured projection data. Since the estimated scatter distributions never contain high frequency structure, this smoothing procedure has little effect on the spatial characteristics of the scatter, thus preserving spatial information while dramatically reducing noise. It is this property of scatter which allows very short two-dimensional studies to be used for the estimation (in conjunction with a higher statistics three-dimensional dataset) of the scatter distribution with this method.

EXPERIMENTAL VALIDATION

Data were acquired using the ECAT-831 (Siemens/CTI, Knoxville, TN) neuro PET scanner. Calculated attenuation corrections (5,6) were applied with the appropriate attenuation coefficients for water, tissue and bone, thus producing accurate, scatter-free attenuation correction factors. Scatter distributions were calculated as de-

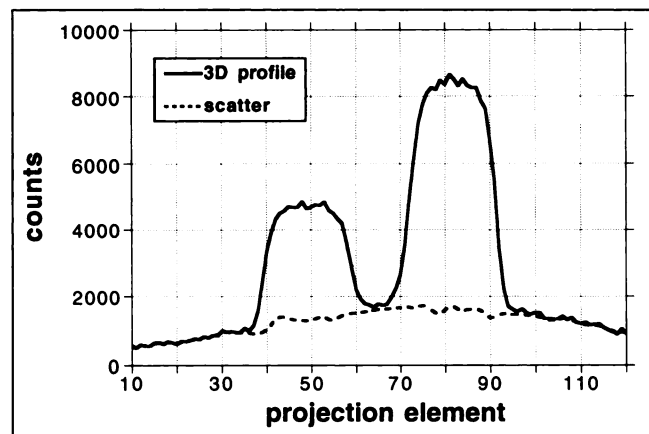


FIGURE 6. Scatter estimate for projection through slot phantom after correction for efficiency and scaling to account for two-dimensional scatter.

scribed above and the corrected three-dimensional datasets reconstructed using a fully three-dimensional algorithm (18–20). All reconstructions, whether two- or three-dimensional, used a Shepp-Logan filter rolled off at the Nyquist frequency which led to a reconstructed image resolution of 6.2 mm at the center of the field of view.

Slot Phantom

This dataset consisted of sequentially acquired two- and three-dimensional scans of 20 min each. The two-dimensional study was acquired as 4×5 min frames, which allowed us to investigate the accuracy of scatter correction as a function of the two-dimensional study length. Scatter corrected (using the 20-min two-dimensional study) and uncorrected reconstructions are shown in Figure 7. The removal of scattered events from the central compartment is appreciable. Also note how the activity within activity-containing compartments is more uniform after scatter correction. To examine improvements in quantitation, regions of interest (ROIs) were placed over the three phantom compartments and activity ratios (left compartment normalized to 1.0) were calculated for the three-dimensional dataset with and without correction and the two-dimensional dataset. We also performed a simple scatter correction on the three-dimensional dataset by fitting a second order polynomial to the tails of each one-dimensional projection in order to assess how well a very simple scatter correction performs. The results demonstrate improving quantitation as scatter is removed (Table 1). The difference method leads to quantitation which is superior to two-dimensional studies without scatter correction. Although the accuracy of the scatter correction is best for two-dimensional data acquired over 20 min, a short 5-min two-dimensional dataset also leads to acceptable results. This is important if

TABLE 1
Activity Ratios in the Slot Phantom for Scatter-Corrected and Uncorrected Datasets

Dataset	Normalized ratio
True ratio	1.00:0.00:2.20
Two-dimensional uncorrected imaging	1.00:0.14:2.11
Three-dimensional uncorrected imaging	1.00:0.37:1.90
Three-dimensional corrected with polynomial imaging	1.00:0.13:2.12
Three-dimensional corrected with 20 min of two-dimensional imaging	1.00:–0.01:2.23
Three-dimensional corrected with 5 min of two-dimensional imaging	1.00:0.03:2.19

the method is to be applied to scatter correction in human three-dimensional studies where the biological redistribution of activity can make time an important factor.

Nonuniform Phantom

The slot phantom is a somewhat idealized case because it contains no inhomogeneities in the attenuating medium and is completely uniform in the axial direction. It can also be misleading to look at activity ratios instead of absolute activity values. In order to validate the method in a more general imaging situation, we used a 20-cm diameter cylinder containing smaller cylinders which were combined to generate activity and attenuating media distributions which were nonuniform both axially and transaxially. The phantom configuration is shown in Figure 8. Sequential 5-min two-dimensional and 20-min three-dimensional studies were acquired. The scatter distribution was determined as previously described and used to correct the three-dimensional projection data. In order to calibrate the three-dimensional PET images for absolute activity, a small 3-cm diameter by 3-cm high cylinder (very low scatter) which contained a known activity concentration was scanned. Attenuation correction in both the calibration source and the phantom study was based on a calculated correction, giving scatter-free correction factors. For the nonuniform phantom, this was achieved by segmenting a transmission scan image of the phantom, assigning the correct narrow-beam μ values (0.095 cm^{-1} for water, 0 cm^{-1} for air) and forward-projecting the full three-dimensional dataset (21). Reconstructed images were calibrated (using ROI counts from the small reconstructed cylinder) and compared to the actual activity concentration with and without scatter correction to determine the improvement in quantitation.

The reconstructed images are shown in Figure 9 with activity concentrations from ROI analysis shown in Table 2. After scatter correction, the images accurately reflect the activity levels in the phantom. The quantitative error is reduced from 30% to 5% in the hot spot and from 48% to 7% in the background. In cold regions, the activity is restored close to zero after scatter correction in both the water cylinder and the air cylinder. It is interesting to

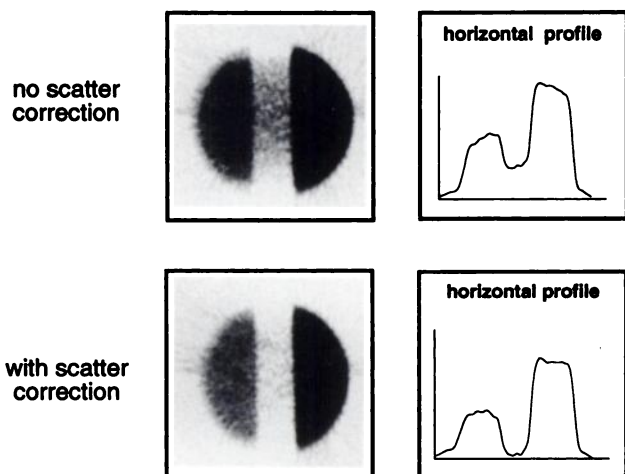


FIGURE 7. Full three-dimensional reconstructions of slot phantom with and without scatter correction. After scatter correction, counts in the central empty compartment have been effectively removed and the profile across the active regions is more uniform.

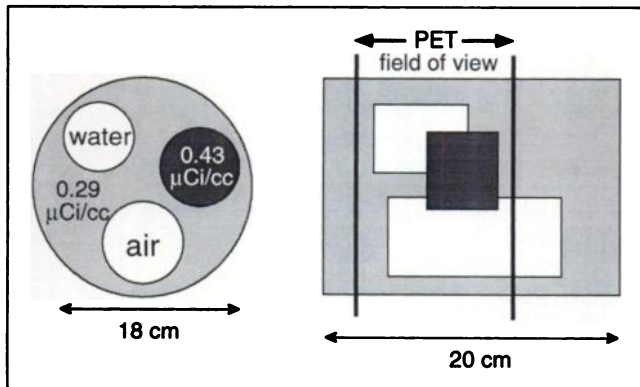


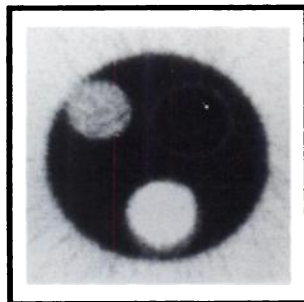
FIGURE 8. Phantom configuration used for absolute quantitative assessment of activity concentration with three-dimensional PET. The phantom is nonuniform in activity and attenuating media distributions both transaxially and in the axial direction.

note how the presence of scatter results in an overestimation of activity in cold regions which have attenuation coefficients similar to water, but an underestimation in regions which have low attenuation coefficients in the range of air. This indicates a preferential redistribution of counts by the filtered backprojection algorithm into areas of high attenuation in the presence of scatter.

Clinical FDG Study

The major prerequisites for using this method for scatter correction in human studies are that activity distribu-

no scatter
correction



with scatter
correction

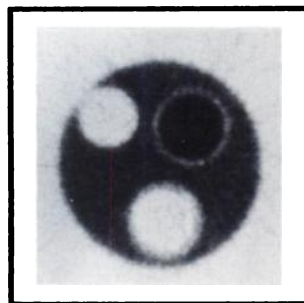


FIGURE 9. Full three-dimensional reconstructions of the non-uniform phantom with and without scatter correction. After correction, the absolute activities are within $0.02 \mu\text{Ci/cc}$ of their correct value when compared to an error of up to $0.14 \mu\text{Ci/cc}$ without scatter correction.

TABLE 2

Absolute Activity Concentrations in Nonuniform Phantom with and Without Scatter Correction

Compartment	Phantom activity $\mu\text{Ci/cc}$	Without correction $\mu\text{Ci/cc}$	Scatter corrected $\mu\text{Ci/cc}$
Background	0.293	0.432 ± 0.023	0.308 ± 0.021
Hot	0.430	0.562 ± 0.022	0.452 ± 0.024
Cold (water)	0.000	0.092 ± 0.021	0.006 ± 0.009
Cold (air)	0.000	-0.019 ± 0.010	0.011 ± 0.012

tion remains static throughout the duration of the scan and that a short two-dimensional study (≈ 5 min) can be used to perform scatter correction. Very slowly changing distributions are encountered in many PET studies (for example, ^{18}F -FDG brain and heart studies and ^{13}N -ammonia blood flow studies where imaging commences after the initial uptake period and the later phases of receptor ligand studies). We illustrate how the method can be applied in human studies using a typical brain ^{18}F -FDG study. A dose of ^{18}F -FDG (10 mCi) was injected into a healthy male volunteer who had given informed consent under the guidelines set by the UCLA Human Subject Protection Committee. A 40-min two-dimensional study (8×5 min) was acquired following a 40-min uptake period. Subsequently, the septa were removed and a 15-min three-dimensional study acquired. The last frame of the two-dimensional study (5 min) was used in the scatter correction procedure. Thus, the total imaging time for the scatter-corrected three-dimensional study was 20 min. Calculated attenuation corrections based on the edges of the sinograms and an assumed skull thickness were applied to the sinograms (6) and the datasets were reconstructed to give the images shown in Figure 10.

Identical ROIs placed over areas containing predominantly gray or white matter (same regions used for all studies) reveal gray-to-white matter ratios of 2.1 (three-dimensional uncorrected image), 3.2 (two-dimensional uncorrected image) and 4.3 (three-dimensional scatter-corrected image). The corrected three-dimensional images show improved contrast and comparable signal-to-noise (S/N) for half the total imaging time of the two-dimensional study. There are no artifacts introduced into images as a result of the scatter correction. These results have direct relevance to many clinical PET procedures as they indicate that improved quantitation can be achieved for a shorter total imaging time using three-dimensional acquisition and reconstruction with a short two-dimensional scan for scatter correction.

DISCUSSION AND CONCLUSION

The difference method is a fast and straightforward technique, based upon direct measurement, for estimating the scatter distribution in three-dimensional PET studies acquired on scanners with retractable septa. It

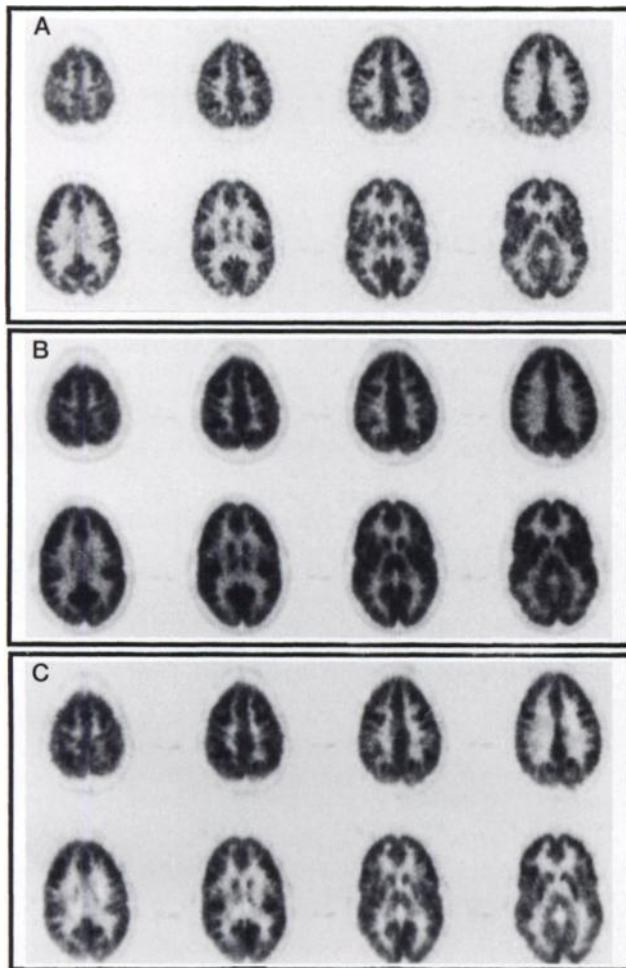


FIGURE 10. Example of scatter correction in a human ^{18}F -FDG study. The 20-min scatter-corrected three-dimensional images (C) show improved contrast over the uncorrected three-dimensional images (B) while retaining similar S/N characteristics as the two-dimensional study (A) which had an acquisition time of twice as long.

takes into account the spatial distributions of the activity and attenuating medium and includes scatter from activity outside the field of view. This method will be used with phantoms to explore how the scatter distribution changes as a function of the size, shape and distribution of the source and the scattering medium. For some in vivo PET imaging procedures, it can also be used to perform a scatter correction. This necessitates an additional short two-dimensional scan which is easily incorporated into the imaging protocol on scanners which have mechanically retractable septa. Absolute quantitation within 10% has been demonstrated in a very general imaging situation using an additional two-dimensional scan of just 5 min. Noise propagation can be reduced by smoothing the scatter data before subtraction.

ECAT-831 datasets consist of sinograms with dimensions of 128×160 . The two- and three-dimensional datasets consist of 15 and 64 of these sinograms respectively.

The difference method has been written in FORTRAN and requires approximately 3 min CPU time on a VAX 3200 workstation (DEC, Maynard, MA). On the same hardware, the full three-dimensional reconstruction (image size $128 \times 128 \times 15$) takes 1.2 hr; thus, the extra computation involved in scatter correction would be minimal. Using i860-based workstation accelerator boards, we have now achieved three-dimensional reconstruction times of 5 min (Guerrero TM, *personal communication*). A similar speed-up of the scatter correction algorithm can be expected on this hardware, allowing a complete three-dimensional dataset from the ECAT-831 to be corrected for scatter and reconstructed in under 6 min. We anticipate further improvements in the algorithm. In particular, the extension of the direct plane scatter data to oblique LORs may benefit from a more involved approach compared with the current method of linear interpolation, especially with scanners employing larger axial acceptance angles.

If the difference method is used to characterize scatter, care must be taken in the interpretation of the resulting scatter distributions. With this method (as with the dual energy technique), very small errors in the normalization of the two datasets to be subtracted will lead to apparent structure (closely related to the source distribution) in the scatter estimate. Motion between the two- and three-dimensional studies could also cause such artifacts. The appearance of such structure should be interpreted carefully.

We have validated the approximations and assumptions of this method for our particular scanner geometry. Two parameters which may influence the success of this method are the maximum axial acceptance angle of the scanner and the energy window utilized. On more modern scanners which have improved energy resolution, it is common to set the lower threshold between 350–380 keV. This may result in differences between the shape of the two- and three-dimensional scatter distributions. This point will require further investigation.

The results of the FDG study in combination with the phantom experiments argue strongly for the use of three-dimensional PET with scatter correction for FDG clinical brain studies. If calculated attenuation correction is used, high quality images (defined by contrast, resolution and quantitative accuracy) can be obtained for a total imaging time of 20 min, thus permitting improved patient throughput for these studies. Alternatively, the S/N advantages of three-dimensional acquisition can be realized while retaining (or even improving) on the quantitative accuracy of two-dimensional images for a similar total imaging time. Similar benefits are likely for other clinical PET studies, although each case must be judged separately due to the dependence of the S/N gain in three-dimensional studies on injected dose, count-rate capability and the sensitivity increase due to septa removal (3). Even with a relatively noise-free scatter correction, there will be some reduction in S/N. The images in Figure 10 and the

ROI data for the nonuniform cylinder (Table 2) indicate that these losses are relatively small compared with the large gain achieved by three-dimensional data acquisition.

If the scatter distribution is fairly insensitive to source distributions (preliminary data suggest this might be the case), then the method may even work for dynamic studies. Here, the two-dimensional scan can be performed in the latter stages of the study when the tracer distribution is changing slowly and the resulting scatter correction applied back to data acquired in the early, rapidly changing phase.

In conclusion, the difference method consistently removes over 90% of the total scatter in three-dimensional PET studies without producing any visible artifacts, thus substantially improving image quantitation and contrast and maintaining the majority of the signal-to-noise benefits of three-dimensional acquisition.

ACKNOWLEDGMENTS

The authors thank Paul Marsden, Stefan Siegel, Lars Eriksson and Magnus Dahlbom for helpful discussions; Roger Woods for providing the human subject data; Ron Sumida, Geoff Currie, Francine Aquilar and Larry Pang for technical assistance; Diane Martin for help with the illustrations; Ken Meadors for phantom construction and the staff of the cyclotron for the preparation of isotopes. This work was presented in part at the 39th Annual Meeting of the Society of Nuclear Medicine, 1992, Los Angeles, CA and was supported by Department of Energy Contract DEFC03-87ER 60615 and NCI grant R01-CA56655.

REFERENCES

1. Dahlbom M, Eriksson L, Rosenqvist G, Bohm C. A study of the possibility of using multi-slice PET systems for three-dimensional imaging. *IEEE Trans Nucl Sci* 1989;NS-36:1066-1071.
2. Townsend DW, Spinks T, Jones T, et al. Three dimensional reconstruction of PET data from a multi-ring camera. *IEEE Trans Nucl Sci* 1989; 36:1056-1065.
3. Cherry SR, Dahlbom M, Hoffman EJ. Three-dimensional positron emission tomography using a conventional multi-slice tomograph without septa. *J Comput Assist Tomogr* 1991;15:655-668.
4. Ranger NT, Thompson CJ, Evans AC. The application of a masked orbiting transmission source for attenuation correction in PET. *J Nucl Med* 1989;30:1056-1068.
5. Bergstrom M, Litton J, Eriksson L, Bohm C, Blomqvist G. Determination of object contour from projections for attenuation correction in cranial positron emission tomography. *J Comput Assist Tomogr* 1982;6: 365-372.
6. Siegel S, Dahlbom M. Implementation and evaluation of a calculated attenuation correction for PET. *IEEE Trans Nucl Sci* 1992;39:1117-1121.
7. McKee BTA, Hogan MJ, Howse DCN. Compton scattering in a large-aperture positron imaging system. *IEEE Trans Med Imag* 1988;7:198-202.
8. Barney JS, Rogers JG, Harrop R, Hoverath H. Object shape dependent scatter simulations for PET. *IEEE Trans Nucl Sci* 1991;38:719-725.
9. Michel C, Bol A, Spinks TJ, et al. Assessment of response function in two PET scanners with and without interplane septa. *IEEE Trans Med Imag* 1991;10:240-248.
10. Bergstrom M, Eriksson L, Bohm C, Blomqvist G, Litton J. Correction for scattered radiation in a ring detector positron camera by integral transformation of the projections. *J Comput Assist Tomogr* 1983;7:42-50.
11. Townsend DW, Geissbuhler A, Defrise M, et al. Fully three-dimensional reconstruction for a PET camera with retractable septa. *IEEE Trans Med Imag* 1991;10:505-512.
12. Bailey DL. Three-dimensional acquisition and reconstruction in positron emission tomography. *Ann Nucl Med* 1992;6:123-130.
13. Grootoontk S, Spinks TJ, Jones T, Michel C, Bol A. Correction for scatter using a dual energy window technique with a tomograph operated without septa. *IEEE Conf Record* 1991;3:1569-1573.
14. Barney JS, Harrop R, Rogers JG. Scatter correction for positron volume imaging using analytic simulation. *IEEE Conf Record* 1991;3:2101-2106.
15. Ollinger J. Estimation of the distribution of scattered coincidences in PET using transmission scans [Abstract]. *J Nucl Med* 1991;32:996.
16. Hoffman EJ, Phelps ME, Huang SC, Mazziotta JC, Digby WM, Dahlbom M. A new PET system for high resolution three-dimensional brain imaging. *J Nucl Med* 1987;28:758-759.
17. Hoffman EJ, Digby WM, Germano G, Mazziotta JC, Huang SC, Phelps ME. Performance of a neuroPET system employing two-dimensional modular detectors. *J Nucl Med* 1988;29:983-984.
18. Kinahan PE, Rogers JG. Analytic three-dimensional image reconstruction using all detected events. *IEEE Trans Nucl Sci* 1989;NS-36:964-968.
19. Defrise M, Townsend DW, Geissbuhler A. Implementation of three-dimensional image reconstruction for multi-ring tomographs. *Phys Med Biol* 1990;35:1361-1372.
20. Cherry SR, Dahlbom M, Hoffman EJ. Evaluation of a three-dimensional reconstruction algorithm for multi-slice PET scanners. *Phys Med Biol* 1992;37:779-790.
21. Meikle SR, Dahlbom M, Cherry SR. Attenuation correction using count-limited transmission data in positron emission tomography. *J Nucl Med* 1993;34:143-150.